Available online at www.sciencedirect.com
SCIENCE DIRECT®
Journal of Power Sources 115 (2003) 179–186
JOURNAL OF POWER SOURCES
www.elsevier.com/locate/jpowsour

The optimization of specific capacitance of amorphous manganese oxide for electrochemical supercapacitors using experimental strategies

Chi-Chang Hu*, Ta-Wang Tsou

Department of Chemical Engineering, National Chung Cheng University, Chia-Yi 621, Taiwan, ROC

Received 6 August 2002; received in revised form 21 October 2002; accepted 28 November 2002

Abstract

The optimal deposition conditions for plating the amorphous manganese oxide (denoted as a-$MnO_x{\cdot}nH_2O$) with a maximum specific capacitance were approached by using the experimental strategies, including the fractional factorial design (FFD), the path of steepest ascent and the central composite design (CCD) coupled with the response surface methodology (RSM). The anodic deposition variables such as current density of deposition, pH, $MnSO_4$ concentration and temperature of the plating bath were found to be the key factors influencing the specific capacitance of a-$MnO_x{\cdot}nH_2O$ in the FFD study. These variables were subjected to the path of the steepest ascent study to approach the vicinity of optimal conditions for plating the a-$MnO_x{\cdot}nH_2O$ deposit with a maximum specific capacitance. Effects of the current density and the $MnSO_4$ concentration were further examined using a regression model in the CCD study. This model, represented as response surface contour plots, showed that a-$MnO_x{\cdot}nH_2O$ deposited under pH of 5.6, a current density of 3.7 mA cm^{-2}, a passed charge of 0.3 C cm^{-2}, a $MnSO_4$ concentration of 0.16 M and a deposition temperature of 24 °C exhibited the highest specific capacitance of ca. 220 F g^{-1}.

Keywords: Electrochemical supercapacitors; Amorphous manganese oxide; Specific capacitance; Experimental strategies

1. Introduction

Due to the unique characteristics of the pulse-power property, the excellent reversibility and the longer cyclic life in comparison with batteries [1–3], supercapacitors have attracted much attention of many electrochemists. The promising application fields of supercapacitors include the hybrid electric vehicles, fuel cells, PCS cellular phones, PDA systems, etc. [1–6]. In general, supercapacitors can be divided into two types on the basis of the charge-storage mechanism, principally the capacitance of the electric double layer and the pseudocapacitance of redox reactions at/within the electroactive materials [1–3]. The double-layer capacitors are usually composed of very high surface area electrodes (e.g. carbon fibers) because the non-Faradaic capacitance of the electric double layer is directly proportional to the surface area accessible by electrolytes [3,7]. On the other hand, the electrodes of electrochemical pseudocapacitors mainly consist of electroactive materials with several oxidation states or structures [3,8–10]. Recently, the electrochemical pseudocapacitors have been paid much attention because the capacitive characteristics (e.g. a higher energy density), estimated theoretically, of these devices are better than that of the double-layer capacitors [1,2]. Moreover, supercapacitors with a high pulse-power and an acceptable energy capability are believed to be a potential device in several future applications, such as an energy manager or tuner in the electric power systems [11].

Many researchers focused on developing the electrodes materials, such as transition-metal oxides (e.g. oxides of Mn, Mo, V, Cr, W, Ru, Ir, Ni, Co, etc.) and conducting polymers with several oxidation states/structures for the application of supercapacitors [1–3,8–19]. Although there are several oxidation states, including Mn(0), Mn(II), Mn(III), Mn(IV), Mn(V), Mn(VI), and Mn(VII), for manganese oxides [20], they were often employed as the cathode materials in rechargeable batteries [21,22]. Recently, manganese oxides have been considered as a potential candidate for the electrode material of supercapacitors [14–16,23,24]. In addition, several methods have been developed for preparing manganese oxides, including chemical oxidation [25], sol–gel-derived method [15], chemical coprecipitation [14,16] and electrochemical deposition [22–24,26]. Based on the relatively complicated steps of the other techniques, it is

* Corresponding author. Tel.: +886-5-2720411x33411; fax: +886-5-2721206.
E-mail address: chmhcc@ccu.edu.tw (C.-C. Hu).

0378-7753/03/$ – see front matter © 2003 Elsevier Science B.V. All rights reserved.
doi:10.1016/S0378-7753(02)00647-X

more desirable to employ the electrochemical deposition for preparing the manganese oxides with excellent capacitive characteristics.

Recently, the hydrous manganese oxide with an amorphous structure (denoted as a-$MnO_x{\cdot}nH_2O$) was successfully deposited onto a graphite substrate from $MnSO_4$ solutions with different pH by means of anodic deposition [19,23]. In addition, this oxide was found to exhibit ideally capacitive behavior (i.e. acceptable charge capacity, good electrochemical reversibility and high pulse-power property) in a potential window of 1.0 V in Na_2SO_4 and KCl. The purpose of this work is to identify the optimal deposition conditions for preparing a-$MnO_x{\cdot}nH_2O$ with the highest specific capacitance. The fractional factorial design (FFD) was first employed to efficiently find the key deposition variables influencing the specific capacitance of a-$MnO_x{\cdot}nH_2O$ [27,28]. These key variables were subjected to the path of the steepest ascent investigation in order to approach the vicinity of the optimal conditions for the a-$MnO_x{\cdot}nH_2O$ deposition. The central composite design (CCD) coupled with the response surface methodology (RSM) was used to establish the relationship between the specific capacitance and the deposition variables around the optimal conditions of the a-$MnO_x{\cdot}nH_2O$ preparation [27–29]. Moreover, the morphology and roughness factor of manganese oxide deposits with different specific capacitance were examined by means of an atomic force microscope (AFM).

2. Experimental

The 10 mm × 10 mm × 3 mm graphite supports (Nippon Carbon EG-NPL, N.C.K., Japan) were first abraded with ultrafine SiC paper, degreased in an ultrasonic bath of water for 10 min, then, etched in a 0.5 M H_2SO_4 solution at room temperature (ca. 26 °C) for 10 min, and finally degreased with the ultrasonic bath of water for 30 min. The exposed geometric area of these pretreated supports is equal to 1 cm^2 and the other surface areas were coated with polytetrafluorene ethylene (PTFE) films. After deposition, these PTFE films were removed from the electrodes and the electrodes were doubly degreased with water in an ultrasonic bath. The oxide loading of hydrous oxide-coated electrode is the weight difference of the electrode without PTFE coating before and after the application of oxide growth through a microbalance with an accuracy of 10 μg (Sartorius BP 2100D, Germany). The electrodes before and after the oxide deposition were dried by a cool airflow. Note that the oxide loading of all a-$MnO_x{\cdot}nH_2O$ deposits with 0.3 C cm^{-2} is ranged from 0.20 to 0.25 mg cm^{-2} meanwhile it is between 0.37 and 0.44 mg cm^{-2} for the deposits with 0.6 C cm^{-2}.

The electrochemical deposition and characterization of a-$MnO_x{\cdot}nH_2O$ deposits were performed by means of an electrochemical analyzer system, CHI 633A (CH Instrument, USA). All experiments were carried out in a three-compartment cell. An Ag/AgCl electrode (Argenthal, 3 M KCl, 0.207 V versus SHE at 25 °C) was used as the reference. A piece of platinum gauze with an exposed area of 4 cm^2 was employed as the counter electrode. A Luggin capillary, whose tip was set at a distance of 1–2 mm from the surface of the working electrode, was used to minimize errors due to *iR* drop in the electrolytes. The surface morphology and roughness factor of a-$MnO_x{\cdot}nH_2O$ films were examined through means of an atomic force microscope (Digital Instrument NS3a controller with D3100 stage).

All solutions used in this work were prepared with 18 MΩ cm water produced by a reagent water system (Milli-Q SP, Japan) and all reagents not otherwise specified in this work were Merck, GR. In addition, the electrolyte containing 0.1 M Na_2SO_4, used to study the capacitive behavior of a-$MnO_x{\cdot}nH_2O$, was degassed with purified nitrogen gas before electrochemical measurements and nitrogen was passed over the solution during the measurements. The solution temperature was maintained at 25 °C by means of a water thermostat (HAAKE DC3 and K20).

3. Results and discussion

The electrochemical behavior of a-$MnO_x{\cdot}nH_2O$ was measured in 0.1 M Na_2SO_4 and typical results measured at different scan rates are shown in Fig. 1. In this figure, no obvious redox peak is found on all curves although an increase in currents is visible at potentials positive to ca. 0.85 V on the positive sweeps and a broad reduction peak is clearly observed in the same potential region on the negative sweeps. Note that these CV curves show typical rectangular and symmetric *i–E* responses when electrode potentials are below 0.85 V, indicating the fact that the Faradaic redox reactions occurring at/within the a-$MnO_x{\cdot}nH_2O$ deposit are highly electrochemically reversible. The above results reveal the promising potential of this material in the application of electrochemical supercapacitors. Similar responses with ideally capacitive characteristics have also been found

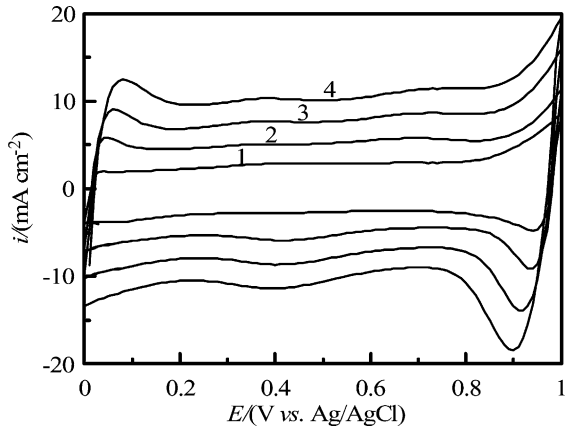

Fig. 1. Cyclic voltammograms of a-$MnO_x{\cdot}nH_2O$ measured in 0.1 M Na_2SO_4 at: (1) 20 mV s^{-1}; (2) 50 mV s^{-1}; (3) 75 mV s^{-1}; and (4) 100 mV s^{-1}.

for a-$MnO_x{\cdot}nH_2O$ prepared by a potentiostatic method from similar solutions [19,23], implying that the electrochemical characteristics of a-$MnO_x{\cdot}nH_2O$ plated by the anodic deposition are not significantly influenced by the plating modes. Also note that the shape of these voltammetric curves was not influenced by changing the scan rate of CV from 20 to 100 mV s^{-1}. In addition, voltammetric currents were directly proportional to the scan rate of CV, indicating the ideally capacitive performance. The mean specific capacitance (C_S) of a-$MnO_x{\cdot}nH_2O$ can be estimated on the basis of the following equation [8–10,18,19,23]:

$$C_S = \frac{\text{voltammetric charge}}{\text{potential window} \times \text{oxide loading}} = \frac{q^*}{\Delta V \times w} \quad (1)$$

where q^* is integrated from the positive or negative sweeps of CV within the potential window. Due to the increase in voltammetric currents at potentials positive to 0.85 V on the CV curves in Fig. 1, the potential window for the calculation of specific capacitance in this work is set between 0 and 0.85 V. On the basis of Eq. (1), the mean specific capacitance of a-$MnO_x{\cdot}nH_2O$ estimated from curves 1 to 4 in this figure is ranged from ca. 190 to 160 F g^{-1}, respectively. This relatively small difference in specific capacitance indicates the excellent pulse charge–discharge characteristics of a-$MnO_x{\cdot}nH_2O$ plated by anodic deposition, which is very suitable for the supercapacitor application. Note that C_S is employed as the response variable to be optimized in this work.

3.1. Fractional factorial design

A fractional factorial design is employed to efficiently screen out the key variables significantly affecting the specific capacitance of a-$MnO_x{\cdot}nH_2O$. In this experiment design, the influence of each deposition variable on C_S of a-$MnO_x{\cdot}nH_2O$ can be isolated at a variety of other variable levels, as well as the interactions among these variables because a system or process is likely to be driven primarily by some of main factors and low-order interactions [27,28].

The effects of the following deposition variables on the specific capacitance of a-$MnO_x{\cdot}nH_2O$ are investigated in the FFD study: pH of the plating bath (A), current density (B), passed charge (i.e. oxide loading) (C), Mn^{2+} concentration (D) and deposition temperature (E). The fixed levels of these five variables are given in Table 1 where the low and high levels of A, B, C, D, and E are denoted as "−" and "+", respectively. The 2^{5-1} design matrix with levels and the results of specific capacitance (C_S) for various a-$MnO_x{\cdot}nH_2O$ deposits are shown in Table 2. Note that a 2^{k-1} fractional factorial design matrix can be constructed by writing down a basic design matrix consisting of a full 2^{k-1} factorial design and then adding the kth factor by identifying its high (plus) and low (minus) levels through the plus and minus signs of the highest-order interaction $ABC\cdots(K-1)$. For example, the high and low levels of factor E in a 2^{5-1} fractional factorial design can be deduced from the defining relation $I = ABCDE$ (introduced by Box et al. [27]):

$$E = EI = E(ABCDE) = ABCDE^2 = ABCD \quad (2)$$

Therefore, the 2^{5-1} fractional factorial design is obtained by writing down the full 2^4 factorial matrix as the basic design (i.e. columns 2–5 of Table 2) and then equating factor E to the $ABCD$ interaction (i.e. column 6) [28]. According to the defined relationship, the combination of observations used to estimate the effect of the main factor A (pH) is identical to that used to estimate the four-factor interaction effect of the aliases B (current density), C (passed charge), D (Mn^{2+} concentration) and E (deposition temperature). Thus, the main effect of factor A and the interaction effect of $BCDE$ are said to be confounded [27,28]. Based on the principle of the sparsity of effects [28], a system is likely to be driven primarily by the effects of some factors and low-order interactions. Accordingly, effects of the high-order (e.g. three and greater order) interactions are assumed to be negligible and thus, the main effect of factor A can be isolated from the confounded effects by this FFD experiment. Similar situations are also held for factors B, C, D and E. Hence, this FFD study is defined as a design with resolution V [28].

Table 1
Factors and levels for a 2^{5-1} fractional factorial design

Factor	Level	
	+	−
pH (A)	6	4
Current density (B) (mA cm^{-2})	4	1
Passed charge (C) (C cm^{-2})	0.6	0.3
$MnSO_4$ concentration (D) (M)	0.5	0.1
Deposition temperature (E) (°C)	40	20

Table 2
Design matrix and experimental data of specific capacitance (C_S) for depositing a-$MnO_x{\cdot}nH_2O$ in a 2^{5-1} fractional factorial design with the defining relation $I = ABCDE$

Run	Factor					C_S (F g^{-1})
	A	B	C	D	E	
1	−	−	−	−	+	150
2	+	−	−	−	−	191
3	−	+	−	−	−	200
4	+	+	−	−	+	185
5	−	−	+	−	−	180
6	+	−	+	−	+	173
7	−	+	+	−	+	164
8	+	+	+	−	−	193
9	−	−	−	+	−	124
10	+	−	−	+	+	157
11	−	+	−	+	+	157
12	+	+	−	+	−	180
13	−	−	+	+	+	163
14	+	−	+	+	−	173
15	−	+	+	+	−	184
16	+	+	+	+	+	179

Table 3
Analysis of variance for the specific capacitance from the 2^{5-1} fractional factorial design

Source	SS	d.f.	MS	F^*
A	745.6	1	745.6	6.04
B	1072.6	1	1072.6	8.68
D	885.1	1	885.1	7.17
E	588.1	1	588.1	4.76
CD	588.1	1	588.1	4.76
DE	473.1	1	473.1	3.83
Error	1111.6	9	123.5	
Total	5460.9	15		

$R^2 = 1 - (\mathrm{SSE}/\mathrm{SST}) = 0.80$; $F_{0.1}(1,9) = 3.36$.

The C_S data shown in Table 2 are subjected to the analysis of variance (ANOVA) and the result of the statistical analysis is summarized in Table 3. The concept of analysis of variance is based on partitioning the total variability (SST) into its component parts (i.e. model sum of square, $\mathrm{SS_{model}}$, and error sum of square, SSE) [27–29]. Note that SS_i indicates the sum of square corresponding to factor or interaction i. The sum of SS_i with statistical significance is defined as $\mathrm{SS_{model}}$. The quantities $\mathrm{MS}_i = \mathrm{SS}_i/\mathrm{d.f.}_i$ and $\mathrm{MSE} = \mathrm{SSE}/\mathrm{d.f.}_{\mathrm{error}}$ are defined as the mean square of factor (or interaction) i and the mean square of error, respectively. The $\mathrm{d.f.}_i$ and $\mathrm{d.f.}_{\mathrm{error}}$ indicate the degree of freedom for factor i and error, respectively. In Table 3, the test statistics, F^*, defined as $\mathrm{MS}_i/\mathrm{MSE}$, are employed to test the statistical significance of each factor and the two-factor interactions. If the calculated value of F is greater than that in the F distribution table at a specific probability level (e.g. $F_{0.1}(1,9) = 3.36$), a statistically significant factor or interaction is obtained. After the test, factors *A*, *B*, *D* and *E*, and interactions *CD* and *DE* exhibit statistically significant effects on the specific capacitance of a-$MnO_x{\cdot}nH_2O$. In addition, from the calculated F^* values in Table 3, the sequence of factors or interactions with respect to decreasing the statistical significance on C_S is: $B > D > A > E \approx CD > DE$. The other nine effects (including main factor *C* and the other two-factor interactions) without statistical significance are pooled into the error term. The multiple correlation coefficient, $R^2 = 1 - (SSE/SST)$, is the proportion of SST (sum of squares of total variances) explained by the fitted equation. A R^2 value close to 1 means a good fit to the experiment data ($R^2 = 0.80$ in this work).

Calculation of the estimates for main factors and two-factor interactions follows the procedure recommended by Box et al. [27]. The results of all main factors and the two-factor interactions with statistical significance are respectively shown in Fig. 2a and b. In Fig. 2a, main factors *A*, *B* and *C* exhibit positive effects on C_S although factor *C* is statistically insignificant. The above results indicate that the increase in pH of the deposition bath (factor *A*) and the current density of deposition (factor *B*) should increase the specific capacitance of a-$MnO_x{\cdot}nH_2O$. Consequently, a decrease in *D* ($MnSO_4$ concentration) and *E* (deposition temperature) will also increase C_S of a-$MnO_x{\cdot}nH_2O$ deposits. Factor *B* has the largest effect, indicating that the current density has the largest influence on C_S of a-$MnO_x{\cdot}nH_2O$ plating through means of the anodic deposition. In addition, the positive effect of factor *B* is likely due to the increase in roughness for the deposit plated at a high current density since C_S of a-$MnO_x{\cdot}nH_2O$ is found to be directly proportional to its roughness factor (see Section 3.4). A similar situation is applicable for the positive effect of factor *A* as well as the negative effect of factors *D* and *E* since the redox behavior of a-$MnO_x{\cdot}nH_2O$ is insignificantly influenced by varying the deposition settings of all variables investigated in this work. Similar results for the a-$MnO_x{\cdot}nH_2O$ deposits anodically plated by a potentiostatic mode with pH of the plating baths varying from 1.0 to 6.4 have been previously found [19,23], further supporting the above statement.

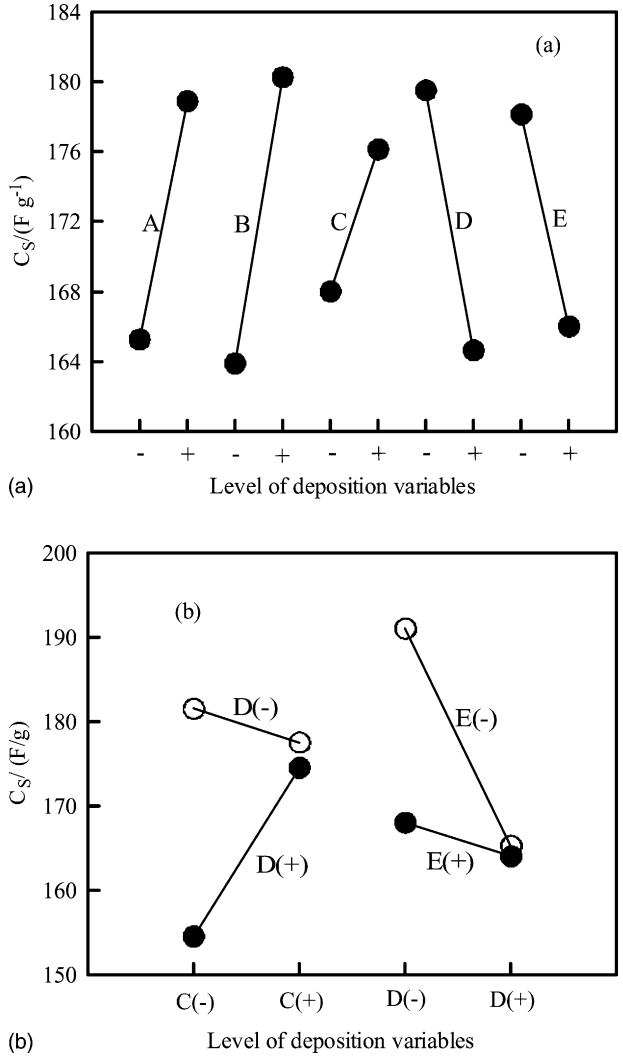

Fig. 2. (a) The effects of main factors: pH (*A*), current density (*B*), passed charge (*C*), $MnSO_4$ concentration (*D*) and temperature (*E*); and (b) the effects of two-factor interactions with statistical significance on the specific capacitance of a-$MnO_x{\cdot}nH_2O$ in the FFD study. Here (+) and (−) indicate the high and low levels of the these factors, respectively.

In Fig. 2b, factor C (oxide loading) exhibits no effect on the specific capacitance of a-$MnO_x{\cdot}nH_2O$ when factor D ($MnSO_4$ concentration) is under the low level. However, an increase in C_S with increasing the oxide loading is clearly found when the $MnSO_4$ concentration is under the high level (i.e. 0.5 M). Hence, there should exist a strong interaction between factors C and D. A similar situation is obvious for the DE interaction. Based on the above results and discussion, a combination of a positive movement in factors A and B and a negative adjustment in factor D and E should obviously increase the specific capacitance of a-$MnO_x{\cdot}nH_2O$.

3.2. Path of steepest ascent

From the analysis of variance and regression analysis of the results shown in Table 2, a fitted polynomial model can be generated. This model, quantitatively elucidating the effects of all plating variables with statistical significance, is expressed in the following:

$$y = 172.06 + 6.81x_A + 8.91x_B - 7.44x_D - 6.06x_E + 6.06x_Cx_D + 5.44x_Dx_E \quad (3)$$

where x_i are the coded variables for factor i (i.e. A, B, C, D and E). The coded variables, x_i, are defined in the standardized form as follow [29]:

$$x_{i,\mathrm{HIGH}} = \frac{X_{i,\mathrm{HIGH}} - X_{i,\mathrm{MEAN}}}{S_i(=+1)} = +1 \quad (4)$$

$$x_{i,\mathrm{LOW}} = \frac{X_{i,\mathrm{LOW}} - X_{i,\mathrm{MEAN}}}{S_i(=-1)} = -1 \quad (5)$$

$$X_{i,\mathrm{MEAN}} = \tfrac{1}{2}(X_{i,\mathrm{HIGH}} + X_{i,\mathrm{LOW}}) \quad (6)$$

$$S_i = \tfrac{1}{2}(X_{i,\mathrm{HIGH}} - X_{i,\mathrm{LOW}}) \quad (7)$$

where $X_{i,\mathrm{HIGH}}$ and $X_{i,\mathrm{LOW}}$ are the high and low levels of factor i in natural units, respectively. Note that factors A, B, D and E are considered in the steepest ascent study from the Section 3.1. From Eq. (3), the sign of coefficients for factors A and B is positive while that of factors D and E is negative. On the other hand, from the results and discussion for Fig. 2b, a synergistic effect on increasing the specific capacitance of a-$MnO_x{\cdot}nH_2O$ deposits should occur when factors D and E are simultaneously moved in the negative direction. In addition, C_S of a-$MnO_x{\cdot}nH_2O$ should also be increased if factors A and B are moved in the positive direction. Accordingly, both factors A and B have to be moved in the positive direction while factors D and E have to be moved in the negative direction to reach the vicinity of optimal conditions for plating a-$MnO_x{\cdot}nH_2O$. Moreover, factor C has to be kept under the low level in order to have a synergistic effect on C_S of a-$MnO_x{\cdot}nH_2O$ since factor D has to be moved in the negative direction.

The path of the steepest ascent is the direction in which the response variable(s) increase most rapidly, which is directly proportional to the regression coefficients of the control variables in Eq. (3). Thus, the step size along the steepest ascent path is approximately proportional to the first-order regression coefficients [27–29]. Note that factor C is not considered in this study of the steepest ascent path since the passed charge (i.e. oxide loading) is an insignificant effect and it has to be kept under the low level. Thus, based on Eq. (3) and the above methodology, the direction of the steepest ascent path should be simultaneously moved $+6.81S_A$, $+8.19S_B$, and $-7.44S_D$ in the x_A, x_B and x_D directions, respectively for every $-6.06S_E$ in the x_E direction. Accordingly, the step sizes of factors A (pH), B (current density), D ($MnSO_4$ concentration) and E (temperature) are $+0.3$, $+0.6$ mA, -0.07 M and -3 °C, respectively. Typical points on the path of the steepest ascent study with the corresponding results are shown in Table 4. From Table 4, the experimental settings of run 3 should be located around the vicinity of the optimal conditions for the highest specific capacitance of a-$MnO_x{\cdot}nH_2O$. Since C_S reaches the maximum under the experimental settings of run 3, the experimental settings of run 3 are suitable for the central composite design study coupled with the response surface methodology [27–29]. Therefore, the optimal plating settings for the highest C_S of a-$MnO_x{\cdot}nH_2O$ ought to be obtained from the CCD study carried out in Section 3.3.

Table 4
Points and the results of specific capacitance on the path of steepest ascent

Run	Factor					C_S (F g^{-1})
	A	B (mA cm^{-2})	C (C cm^{-2})	D (M)	E (°C)	
1	5.0	2.5	0.3	0.3	30	174
2	5.3	3.1	0.3	0.23	27	186
3	5.6	3.7	0.3	0.16	24	222
4	5.9	4.3	0.3	0.09	21	190
5	6.2	4.9	0.3	0.02	18	183

3.3. Central composite design

The purpose of the central composite design is to provide enough tests to fit the second-order model correlating the deposition variables and the specific capacitance of a-$MnO_x{\cdot}nH_2O$ anodically plated by means of the galvanostatic method. Since the experimental settings of run 3 should be located around the vicinity of the optimal conditions for the highest specific capacitance of a-$MnO_x{\cdot}nH_2O$, the central point of the CCD study is set at run 3. Note that only factors B and D are considered in this study since these two factors exhibit the most significant effects on the specific capacitance from the ANOVA results (see Table 3). Thus, the pH and temperature of plating baths are kept constant (pH = 5.6 and $T = 24$ °C) in the CCD study.

The design matrix with the corresponding results in the CCD study is shown in Table 5. Note that in this design, the distance from the other experimental points to the central points is constant ($\sqrt{2}$ units). A design with this property will leave a constant variance of the response variable at all

Table 5
Design matrix and experimental data of the specific capacitance of a-$MnO_x{\cdot}nH_2O$ deposits in the central composite design with a quadratic form fit

Run	Factor		C_S (F g^{-1})
	B (mA cm^{-2})	D (M)	
1	−1 (3.1)	−1 (0.09)	194
2	−1 (3.1)	+1 (0.23)	203
3	+1 (4.3)	−1 (0.09)	193
4	+1 (4.3)	+1 (0.23)	193
5	0 (3.7)	0 (0.16)	226
6	0 (3.7)	0 (0.16)	223
7	0 (3.7)	0 (0.16)	220
8	0 (3.7)	$-\sqrt{2}$ (0.06)	172
9	0 (3.7)	$+\sqrt{2}$ (0.26)	182
10	$-\sqrt{2}$ (2.85)	0 (0.16)	182
11	$+\sqrt{2}$ (4.55)	0 (0.16)	189

experimental points when the design is rotated about the center [27]. In addition, experiments on the central point are repeated three times in order to evaluated the pure error between each experiment [27]. The regression analysis and analysis of variance for the data shown in Table 5 were carried out and the resultant second-order model representing the dependence of C_S on factors B (current density) and D ($MnSO_4$ concentration) was generated as follow:

$$y = 223 + 2.9x_D - 15.1x_B^2 - 19.4x_D^2 - 2.3x_Bx_D \quad (8)$$

where y, x_B and x_D are indicative of C_S, the current density of deposition and the concentration of $MnSO_4$, respectively. Note the negative signs corresponding to the coefficients of x_B^2 and x_D^2, indicating the existence of a maximum in this CCD study.

The contour plots for the dependence of C_S of a-$MnO_x{\cdot}nH_2O$ in the CCD study on factors B and D were constructed by using the regression model (i.e. Eq. (8)) and a typical contour diagram is shown in Fig. 3. Note that the specific capacitance of a-$MnO_x{\cdot}nH_2O$ deposits reaches a maximum at the central point of the CCD study. In addition, the rate of decreasing C_S is relatively faster in the x_D direction in comparison with that in the x_B direction. Since the maximum C_S value is located within the investigated range of the CCD study, the above results reveal that the optimal deposition settings for plating the a-$MnO_x{\cdot}nH_2O$ deposit with the highest specific capacitance have been obtained from the above sequential experimental strategies, including the FFD, path of the steepest ascent and CCD studies.

3.4. Atomic force microscopic morphologies and roughness

It is interesting to note that the ideally capacitive performance of a-$MnO_x{\cdot}nH_2O$ deposits prepared by anodic deposition is not significantly influenced by varying the deposition variables although the specific capacitance of

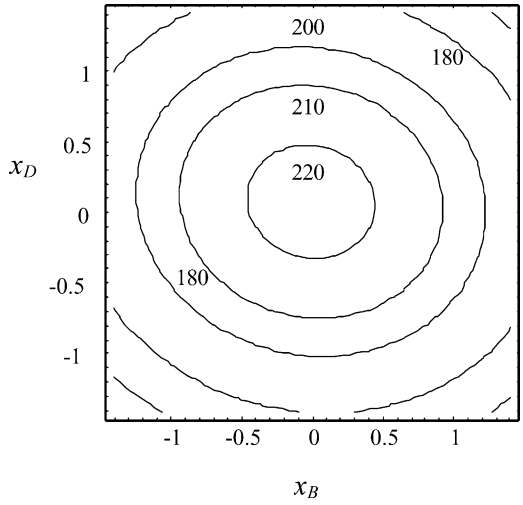

Fig. 3. Contour lines for constant specific capacitance of a-$MnO_x{\cdot}nH_2O$ against the current density of deposition (x_B) and the $MnSO_4$ concentration (x_D) in the CCD study.

this material is strongly dependent upon these variables. Moreover, all deposits prepared in this work exhibit an amorphous structure although the oxide loading has been changed obviously in the FFD study. In order to gain a understanding for the difference between a-$MnO_x{\cdot}nH_2O$ deposits prepared in different conditions, the morphologies and roughness factor (R_q) of three a-$MnO_x{\cdot}nH_2O$ deposits prepared at different conditions with their C_S varying from ca. 120 to 220 F g^{-1} are measured by an atomic force microscope. Typical R_q and C_S data with their preparation conditions are shown in Table 6. In addition, the AFM morphologies of deposits 1–3 in Table 6 are shown in Fig. 4 as photographs 1–3, respectively. In general, the morphology of all a-$MnO_x{\cdot}nH_2O$ deposits shown in Fig. 4 is rough. The highly rough surface should favor the proton inserting into/expelling out the oxide matrix during the redox transitions since the mechanism of energy storage for a-$MnO_x{\cdot}nH_2O$ is believed to be similar to the case of hydrous ruthenium oxide [8,9,30,31], which can be expressed as the following equation:

$$MnO_a(OH)_b + \delta H^+ + \delta e^- = MnO_{a-\delta}(OH)_{b+\delta} \quad (9)$$

where $MnO_a(OH)_b$ and $MnO_{a-\delta}(OH)_{b+\delta}$ indicate interfacial oxy-/hydroxyl-Mn species at higher and lower oxidation states, respectively. In addition, a rougher surface of a deposit should exhibit a larger double-layer capacitance.

Table 6
Experimental settings and data of roughness factor (R_q) and specific capacitance (C_S) for a-$MnO_x{\cdot}nH_2O$

Deposit	Factor					C_S (F g^{-1})	R_q (nm)
	A	B	C	D	E		
1	4	1	0.3	0.5	20	124	536.24
2	5	2.5	0.3	0.3	30	174	563.73
3	5.6	3.7	0.3	0.16	24	222	723.52

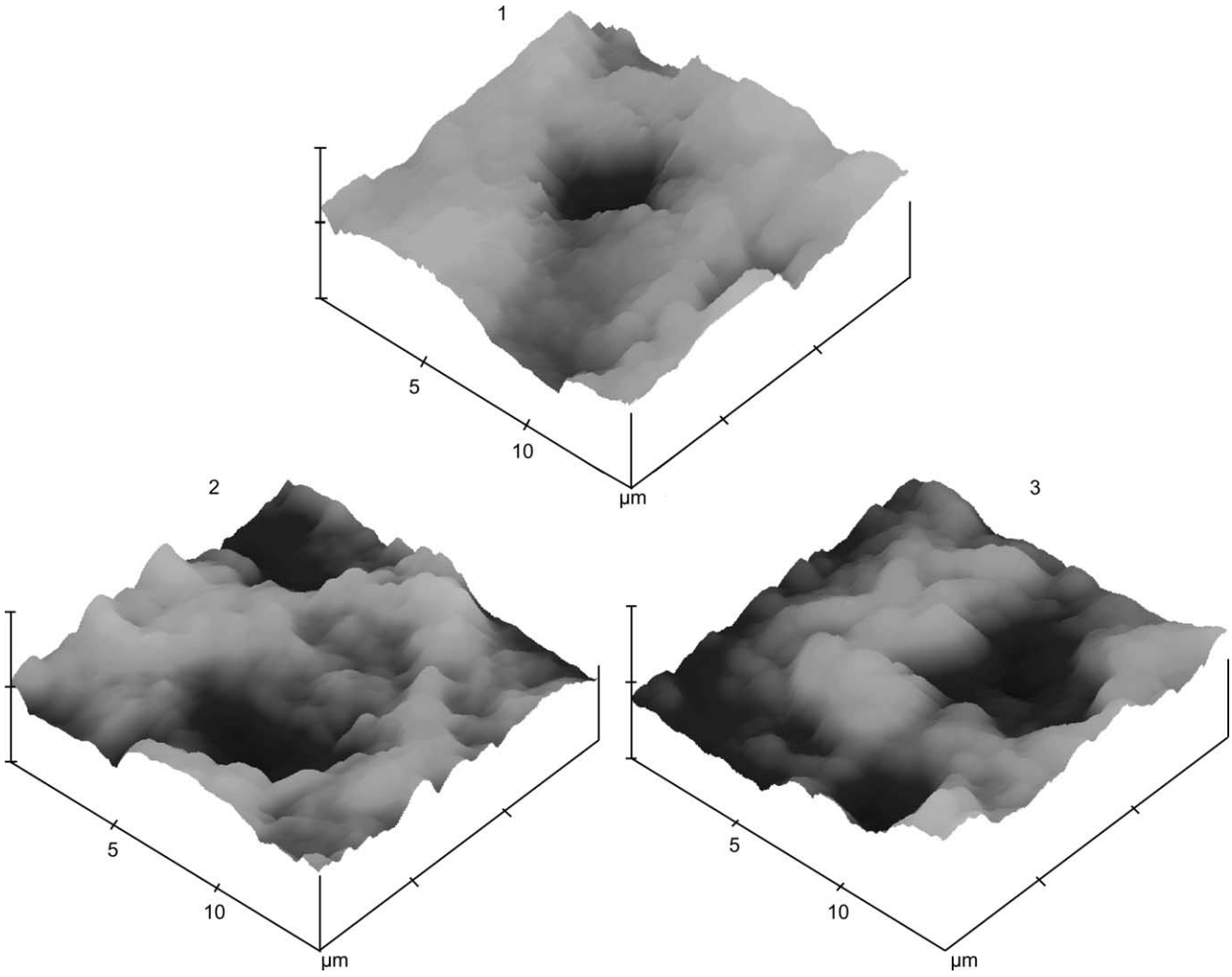

Fig. 4. AFM morphologies of the deposits 1–3 presented in Table 6.

A comparison of the roughness factor obtained from AFM and the specific capacitance of a-$MnO_x{\cdot}nH_2O$ shown in Table 6 indicates that the specific capacitance is proportional to the roughness factor of a-$MnO_x{\cdot}nH_2O$. This result indicates that the electrochemically active surface sites, providing the pseudocapacitance, within the oxide deposits should be proportional to the real surface area of a-$MnO_x{\cdot}nH_2O$ [32–34] since roughness factor is believed to be proportional to the real surface area. This increase in deposit roughness of a-$MnO_x{\cdot}nH_2O$ is attributable to a combination of the increase in pH and the plating current density as well as the decrease in $MnSO_4$ concentrations, especially the current density of deposition since a rougher deposit usually results from a higher current density of deposition [35].

4. Conclusions

The key factors, screened out in the fractional factorial design, influencing the specific capacitance of a-$MnO_x{\cdot}nH_2O$ anodically deposited by the galvanostatic method are the current density of deposition, the concentration of $MnSO_4$, pH and temperature of the plating bath. Using the sequential experiment strategies (i.e. the fractional factorial design, the path of steepest ascent, and the central composite design coupled with response surface methodology), a maximum specific capacitance of 220 F g^{-1} is obtained on the a-$MnO_x{\cdot}nH_2O$ deposit prepared under pH of 5.6, a current density of 3.7 mA, a passed charge of 0.3 C cm^{-2}, a $MnSO_4$ concentration of 0.16 M and a plating temperature of 24 °C. The specific capacitance of a-$MnO_x{\cdot}nH_2O$ was found to be directly proportional to the roughness factor from the AFM analysis.

Acknowledgements

The financial support of this work, by the National Science Council of the Republic of China under contract no. NSC 91-2216-E-194-004, is gratefully acknowledged.

References

[1] A. Burke, J. Power Sources 91 (2000) 37.
[2] R. Kotz, M. Carlen, Electrochim. Acta 45 (2000) 2483.
[3] B.E. Conway, Electrochemical Supercapacitors, Kluwer Academic Publishers, New York, 1999, p. 12.
[4] G. Gutmann, J. Power Sources 84 (1999) 275.
[5] L.P. Jarvis, T.B. Atwater, P.J. Cygan, J. Power Sources 79 (1999) 60.
[6] R.A. Huggins, Solid State Ionics 134 (2000) 179.
[7] A.J. Bard, L.R. Faulkner, Electrochemical Methods, Fundamentals and Applications, Wiley, Singapore, 1980, p. 10.
[8] C.-C. Hu, Y.-H. Huang, J. Electrochem. Soc. 146 (1999) 2465.
[9] C.-C. Hu, K.-H. Chang, Electrochim. Acta 45 (2000) 2685.
[10] C.-C. Hu, C.-H. Chu, J. Electroanal. Chem. 503 (2001) 105.
[11] E. Faggioli, P. Rena, V. Danel, X. Andrieu, R. Mallant, H. Kahlen, J. Power Sources 84 (1999) 261.
[12] C. Lin, J.A. Ritter, B.N. Popov, J. Electrochem. Soc. 145 (1998) 4097.
[13] V. Srinivasan, J.W. Weidner, J. Electrochem. Soc. 144 (1997) L210.
[14] H.Y. Lee, S.W. Kim, H.Y. Lee, Electrochem. Solid State Lett. 4 (2001) A19.
[15] S.-C. Pang, M.A. Anderson, T.W. Chapman, J. Electrochem. Soc. 147 (2000) 444.
[16] H.Y. Lee, J.B. Goodenough, J. Solid State Chem. 144 (1999) 220.
[17] H.Y. Lee, J.B. Goodenough, J. Solid State Chem. 148 (1999) 81.
[18] C.-C. Hu, C.-Y. Cheng, Electrochem. Solid State Lett. 5 (2002) A43.
[19] C.-C. Hu, T.-W. Tsou, Electrochem. Commun. 4 (2002) 105.
[20] M. Pourbaix, Atlas of Electrochemical Equilibria in Aqueous Solutions, National Association of Corrosion Engineers, Houston, TX, 1966, p. 286.
[21] M.M. Doeff, A. Anapolsky, L. Edman, T.J. Richardson, L.C. De Jonghe, J. Electrochem. Soc. 148 (2001) A230.
[22] L.I. Hill, R. Portal, A. Le Gal La Salle, A. Verbaere, D. Guyomard, Electrochem. Solid State Lett. 4 (2001) D1.
[23] C.-C. Hu, T.-W. Tsou, Electrochim. Acta 47 (2002) 3523.
[24] J. Jiang, A. Kucernak, Electrochim. Acta 47 (2002) 2381.
[25] R. Patrice, B. Gerand, J.B. Leriche, L. Seguin, E. Wang, R. Moses, K. Brandt, J.M. Tarascon, J. Electrochem. Soc. 148 (2001) A448.
[26] S. Rodrigues, N. Munichandraiah, A.K. Shukla, J. Appl. Electrochem. 28 (1998) 1235.
[27] G.E.P. Box, W.G. Hunter, J.S. Hunter, Statistics for Experiments, Wiley, New York, 1978, p. 374.
[28] D.C. Montgomery, Design and Analysis of Experiments, fifth ed., Wiley, Singapore, 2001, p. 303.
[29] J.A. Cornell, How to Apply Response Surface Methodology, vol. 8, ASQC, Wisconsin, 1990, p. 3.
[30] C.-C. Hu, Y.-H. Huang, Electrochim. Acta 46 (2001) 3431.
[31] C.-C. Hu, Y.-H. Huang, K.-H. Chang, J. Power Sources 108 (2002) 117.
[32] L.D. Burke, O.J. Murphy, J. Electroanal. Chem. 96 (1979) 19.
[33] H.-J. Heidrich, L. Muller, B.I. Podlovchenko, J. Appl. Electrochem. 20 (1990) 686.
[34] S. Ardizzone, G. Fregonara, S. Trasatti, Electrochim. Acta 35 (1990) 263.
[35] D. Pletcher, F.C. Walsh, Industrial Electrochemistry, second ed., Chapman & Hall, New York, 1990, p. 399.